Stratospheric and Tropospheric Flux Contributions to the Polar Cap Energy Budgets

CHRISTOPHER J. CARDINALE,[a] BRIAN E. J. ROSE,[a] ANDREA L. LANG,[a] AND AARON DONOHOE[b]

[a] *Department of Atmospheric and Environmental Sciences, University at Albany, State University of New York, Albany, New York*

[b] *Applied Physics Laboratory, University of Washington, Seattle, Washington*

(Manuscript received 28 October 2020, in final form 9 February 2021)

ABSTRACT: The flux of moist static energy into the polar regions plays a key role in the energy budget and climate of the polar regions. While usually studied from a vertically integrated perspective (F_{wall}), this analysis examines its vertical structure, using the NASA-MERRA-2 reanalysis to compute climatological and anomalous fluxes of sensible, latent, and potential energy across 70°N and 65°S for the period 1980–2016. The vertical structure of the climatological flux is bimodal, with peaks in the middle to lower troposphere and middle to upper stratosphere. The near-zero flux at the tropopause defines the boundary between stratospheric (F_{strat}) and tropospheric (F_{trop}) contributions to F_{wall}. Especially at 70°N, F_{strat} is found to be important to the climatology and variability of F_{wall}, contributing 20.9 W m^{-2} to F_{wall} (19% of F_{wall}) during the winter and explaining 23% of the variance of F_{wall}. During winter, an anomalous poleward increase in F_{strat} preceding a sudden stratospheric warming is followed by an increase in outgoing longwave radiation anomalies, with little influence on the surface energy budget of the Arctic. Conversely, a majority of the energy input by an anomalous poleward increase in F_{trop} goes toward warming the Arctic surface. Overall, F_{trop} is found to be a better metric than F_{wall} for evaluating the influence of atmospheric circulations on the Arctic surface climate.

KEYWORDS: Arctic; Atmospheric circulation; Energy transport; Stratosphere-troposphere coupling; Energy budget/balance; Interannual variability

1. Introduction

The polar regions are marked by weak annual mean insolation and would be extremely cold were it not for the energetic input into the regions from atmospheric and oceanic energy transport. In the Arctic, poleward of 70°N, the annual average poleward energy flux convergence nearly balances the net radiative deficit of the region (110 W m^{-2}) and is dominated by atmospheric energy flux convergence (100 W m^{-2}), while poleward oceanic energy flux convergence (10 W m^{-2}) is an order of magnitude smaller (e.g., Serreze et al. 2007). The polar cap–averaged atmospheric flux convergence, hereafter F_{wall}, is proportional to the zonally and vertically integrated moist static energy (MSE; sensible heat, latent heat, and geopotential) flux across a boundary defining the polar cap. Improving the estimate and understanding of the fluxes contributing to F_{wall} in the Arctic energy budget has been a recurring goal (e.g., Nakamura and Oort 1988; Serreze et al. 2007; Porter et al. 2010; Mayer et al. 2019).

Using atmospheric reanalyses, the poleward flux of MSE has been linked to variability and long-term changes in Arctic surface and free tropospheric temperatures. On synoptic time scales, anomalies in MSE flux convergence have been linked to changes in Arctic sea ice thickness (D.-S. R. Park et al. 2015; H.-S. Park et al. 2015; Graham et al. 2019) and surface warming (Woods and Caballero 2016) via the following sequence:

1) MSE flux convergence initially increases the moist enthalpy (latent and sensible heat) of the atmospheric column at the pressure level of the anomalous flux [see Eq. (4) in Trenberth and Solomon (1994)].
2) The warm and moist atmosphere subsequently fluxes longwave radiation downward to the surface to initiate surface warming and ice melt.

At cold Arctic temperatures, the latent component of the moist enthalpy storage is small; therefore, the moist enthalpy tendency is very nearly proportional to the temperature tendency.

Linking the poleward atmospheric energy flux to the vertical structure of multidecadal trends in Arctic temperatures, Graversen et al. (2008) found that a significant proportion of the vertical structure of Arctic warming in the summer half-year can be explained by changes in F_{wall} at 60°N. Yang et al. (2010) compared the vertical structure of total and F_{wall}-congruent temperature trends during decades of cooling and warming in the Arctic. Their study concluded that decadal variation of Arctic free troposphere temperature is heavily influenced by changes in the poleward flux of atmospheric energy at 65°N, associated with the changing intensity of the polar meridional circulation cell.

More recent studies using atmospheric reanalyses have linked different components of the poleward energy flux to variability in Arctic surface temperatures. Baggett and Lee (2015) found the winter Arctic warming (at 2 m) associated with planetary-scale waves to be greater and more persistent than the warming associated with synoptic-scale waves. During the planetary wave life cycle, significant convergence of latent and sensible heat fluxes in the Arctic increases the downward longwave radiation, warming the surface (Baggett and Lee 2017). The anomalous energy flux into the Arctic was associated with an amplification of the climatological stationary wave pattern forced by tropical convection in the Pacific warm pool. Graversen and Burtu (2016) also found that Arctic warming was associated with enhanced F_{wall} (especially the latent

Corresponding author: Christopher J. Cardinale, ccardinale@albany.edu

DOI: 10.1175/JCLI-D-20-0722.1

heat component) by planetary-scale waves, whereas F_{wall} by synoptic-scale waves was correlated with an enhanced meridional temperature gradient, and thus anticorrelated with Arctic temperature anomalies.

The impact of F_{wall} on high-latitude climate variability and long-term changes is established; however, the analyses on this topic have focused on fluxes linked to tropospheric circulations, whereas the potential role of the stratosphere in F_{wall} anomalies has not been investigated. It is reasonable to assume that the stratospheric contribution to F_{wall} (F_{strat}) is relatively small compared to the tropospheric contribution (F_{trop}), as the stratosphere is dry and makes up a small percentage of atmospheric mass (10%–30% depending on latitude). However, F_{strat} could be important during periods of anomalous stratospheric conditions, such as sudden stratospheric warming (SSW) events, which can have impacts lasting on the order of months (Kidston et al. 2015). SSW events are known to be associated with large poleward heat flux anomalies at 100 hPa (e.g., Polvani and Waugh 2004). This linkage is suggested by the basic dynamical theory of SSWs (e.g., Limpasuvan et al. 2004), where meridional eddy heat flux is a measurable dynamical proxy for the vertical propagation of planetary wave activity (e.g., Edmon et al. 1980). Deceleration of the stratospheric vortex is accomplished through breaking of these upward-propagating planetary waves (e.g., Matsuno 1971). Thus, there is a long tradition in the stratospheric literature of using lower-stratospheric horizontal eddy heat fluxes as a diagnostic for this coupling between the troposphere and stratosphere (e.g., Polvani and Waugh 2004; Butler et al. 2017). However, the role of F_{strat} in the energy budget of the Arctic polar cap has not been studied as carefully.

Comprehensive studies on the variability of F_{strat} and its contribution to the polar cap energy budget are lacking. Overland and Turet (1994) showed that F_{strat} is a nonnegligible portion of F_{wall} at 70°N [consistent with Fig. 13.10 in Peixoto and Oort (1992)] with a large seasonality and maximum values during the winter (November–March). The vertical structure of F_{wall} reported by Overland and Turet (1994) was calculated from spatially coarse reanalysis data (2.5° × 5° horizontal resolution and 11 vertical levels) and has not been updated using a modern high-resolution reanalysis.

We speculate that F_{strat} variability is only very weakly coupled to polar cap surface temperatures. Positive F_{wall} anomalies cause air temperatures within the polar cap to increase. This warming results in increased longwave emission from the atmosphere, both upward [as outgoing longwave radiation (OLR)] and downward to the surface. The efficiency with which increased F_{wall} warms the surface is intimately tied to the partition of this radiative cooling between the upwelling flux to space and the downwelling flux to the surface. For a polar cap in "radiative-advective equilibrium" (Cronin and Jansen 2016), the surface warming effect decreases monotonically with the vertical height of the advective heat source (i.e., MSE flux convergence). Concentrating the atmospheric heating closer to the surface will result in a larger fraction of the anomalous poleward MSE flux convergence going into surface heating versus longwave emission to space. Thus, the impact on the Arctic surface climate from stratospheric heating ought to be much smaller than the impact of a similar magnitude of tropospheric heating.

Much of the literature reviewed above (e.g., Graversen et al. 2008; Yang et al. 2010; Baggett and Lee 2015; Graversen and Burtu 2016; Baggett and Lee 2017) includes relationships between vertically integrated energy fluxes and the climate of the Arctic polar cap. In this study, we will explicitly separate the stratospheric and tropospheric contributions to the climatology and variability of F_{wall}. The stratospheric component will be linked to the literature on stratospheric variability (e.g., Polvani and Waugh 2004; Butler et al. 2017). Additionally, we will quantify the relationship between F_{wall} and the Arctic surface climate after removing the effects of stratospheric variability.

To characterize the stratospheric and tropospheric contributions to F_{wall} and compare their relative impacts on the Arctic surface climate, the analysis presented considers two key themes and associated research questions:

1) Climatology and variability:
   (i) Using a modern reanalysis, the Modern-Era Retrospective Analysis for Research and Applications, version 2 (MERRA-2), what is the vertical structure of the climatological F_{wall} and can it be cleanly separated into contributions from the troposphere (F_{trop}) and stratosphere (F_{strat})?
   (ii) What is the variability of F_{wall}, F_{strat}, and F_{trop} in both hemispheres?
   (iii) How much of the variance of F_{wall} does F_{strat} distinctly explain?
2) Link to the Arctic climate:
   (i) In MERRA-2, what is the Arctic response following an anomalous poleward increase in F_{wall} when dominated by either F_{strat} or F_{trop}?
   (ii) After removing F_{strat} from F_{wall}, is there a stronger correlation between F_{wall} and warming of the Arctic lower-troposphere?

The data and methods used for this analysis are described in section 2. Theme 1 will be addressed in section 3 of this paper; theme 2 will be addressed in section 4.

2. Data and methods

a. MERRA-2

We use atmospheric winds, temperature, specific humidity, geopotential, radiative fluxes at the top of atmosphere (TOA) and surface, and surface turbulent energy fluxes from the Modern-Era Retrospective Analysis for Research and Applications, version 2 (MERRA-2), the latest atmospheric reanalysis (1980–present) produced by NASA's Global Modeling and Assimilation Office (GMAO). MERRA-2 has a horizontal resolution of 0.5° × 0.625°, 72 vertical levels with output interpolated to 42 pressure levels up to 0.1 hPa, and a temporal resolution of 3 h (GMAO 2015). The period 1980–2016 (37 years) is used in this analysis.

Notable improvements from MERRA to MERRA-2 include assimilation of additional satellite observations, conservation of dry mass, and reduced spurious trends and jumps related to changes in the observing system (Bosilovich et al. 2015). Although many of the updates pertain to tropospheric processes, MERRA-2 improves ozone representation and gravity wave drag parameterization. The general circulation

model (GCM) component uses a cubed-sphere grid, thus eliminating computation instability issues near the poles, which can be important during SSW events where cross-polar flow can occur and for studies of the high latitudes. Information on the initial evaluation of the climate in MERRA-2 can be found in Bosilovich et al. (2015), and information on input observations can be found in McCarty et al. (2016).

b. Contributions to F_{wall}

To calculate the MSE flux and F_{wall}, a method similar to Overland and Turet (1994) is followed. MSE is defined by

$$\text{MSE} = c_p T + gz + L_v q, \tag{1}$$

where c_p is the specific heat of dry air at constant pressure, T is temperature, g is the gravitational acceleration, z is geopotential height, L_v is the latent heat of vaporization for water, and q is specific humidity. The contribution from the kinetic energy is small and has been neglected.

The meridional MSE flux is then vMSE, where v is the meridional component of the wind. The F_{wall} term is defined as the polar cap–averaged MSE flux convergence, equal to the zonally and vertically integrated flux through the bounding latitude divided by the area of the polar cap:

$$F_{\text{wall}} = \frac{C}{2\pi A}\int_0^{2\pi}\int_0^{P_s}(c_p vT + gvz + L_v vq)\frac{d\lambda dp}{g}, \tag{2}$$

where C is the circumference of the latitude defining the polar cap boundary and A is the area polar cap. Terms on the RHS correspond to the flux of sensible heat (SH), geopotential (GP), and latent heat (LH), respectively. Note that F_{wall} is computed instantaneously from the 3-hourly data and averaged monthly and daily to define the climatological fluxes and anomalous F_{wall} events, respectively.

Each component of the MSE flux, namely SH, LH, and GP, can be expanded into an eddy flux (EF), a mean meridional circulation flux (MMC), and a net mass flux (NMF; see appendix A). The NMF has been removed from calculations of F_{wall} due to unphysical high-frequency noise associated with the net atmospheric mass flux into the polar cap. The NMF, by definition, has no vertical structure, meaning the results of this study are not sensitive to this term (see appendix A).

The MSE flux has units of J kg^{-1} m s^{-1}. This flux can be written as the local contribution to the integrated flux convergence in terms of W m^{-2} (100 hPa)$^{-1}$ with a conversion factor of $(C/Ag)10^4$. To recover units of W m^{-2}, flux values are vertically integrated. This conversion factor is used to more explicitly compare the flux between the two hemispheres, since we define the latitude of the polar cap boundary differently in the Northern and Southern Hemisphere. 65°S is used rather than 70°S due to large differences in terrain between the latitudes (about 50% of 70°S is over high Antarctic terrain).

3. Climatology and variability

a. Vertical structure of the poleward MSE flux from 1980 to 2016

Figure 1 shows the vertical structure of the monthly averaged poleward MSE flux across 70°N and 65°S from 1000 to 0.1 hPa for the entire period (1980–2016). We use pressure rather than height as the vertical coordinate in order to visualize contributions from each level to the vertical integral (total convergence). At both latitudes, the level of smallest variability and climatological magnitude is found near 300 hPa, which we define as the boundary between tropospheric and stratospheric fluxes.

Across 70°N, the climatological poleward MSE flux and its variability occurs primarily in two distinct and vertically separated locations in the middle stratosphere and middle to lower troposphere. The climatological MSE flux in the stratosphere across 70°N and its variability is almost exclusively a wintertime phenomenon (cf. Figs. 2b,c). The variability of the stratospheric flux across 65°S is small compared to the stratospheric flux across 70°N. Across 65°S, the MSE flux peaks in the lower troposphere (975–800 hPa) during winter. Interestingly, the seasonality of the MSE flux in the lower-troposphere is more pronounced at 65°S than its counterpart at 70°N despite the weaker seasonality of both the magnitude and location of the storm track in the Southern Ocean (Trenberth 1991); this issue is further explored in section 3b.

b. Seasonality of the MSE flux

Annual, winter, and summer means of the MSE flux and its components are shown in Fig. 2. For all results, we use the November–March (NDJFM) winter season and June–August (JJA) summer season in the Northern Hemisphere and the May–September (MJJAS) winter season and December–February (DJF) summer season in the Southern Hemisphere. We use a 5-month winter season for direct comparisons with Overland and Turet (1994) and to identify all sudden stratospheric warming events (Polvani and Waugh 2004). Across 70°N, local poleward maxima in the annual and winter mean MSE flux are located around 30 hPa and in the broad region of the lower and middle troposphere. During the summer, the tropospheric maximum is closer to the surface and the maximum in the stratosphere is an order of magnitude smaller in value and closer to the tropopause. Across 65°S, local poleward maxima in the annual and winter mean MSE flux are located around 150 and 950 hPa. Evidence of a clean separation between tropospheric and stratospheric fluxes are clearly shown, especially during winter, by the minimum in flux magnitude and standard deviation near 300 hPa.

Flux values across 70°N and 65°S are directly compared in units of J kg^{-1} m s^{-1}, with units of W m^{-2} (100 hPa)$^{-1}$, the local polar cap convergence, used when comparing their impact on the climate of the polar regions. The most apparent difference between the hemispheres is in the stratosphere, where the flux convergence at 70°N is much larger than at 65°S both in the annual and winter mean (about 4 times larger in the winter mean). The seasonality of the tropospheric flux across 70°N is much weaker than across 65°S (Fig. 3), especially in the lower troposphere (Fig. 2). Part of this difference can be explained by the trade-off between SH and LH fluxes, which are out of phase at 70°N (cf. green and cyan lines in Fig. 3) but are in phase at 65°S.

These results are consistent with Overland and Turet (1994) for the flux across 70°N. The vertical structure of the MSE flux is generally in agreement, except for the magnitude of the

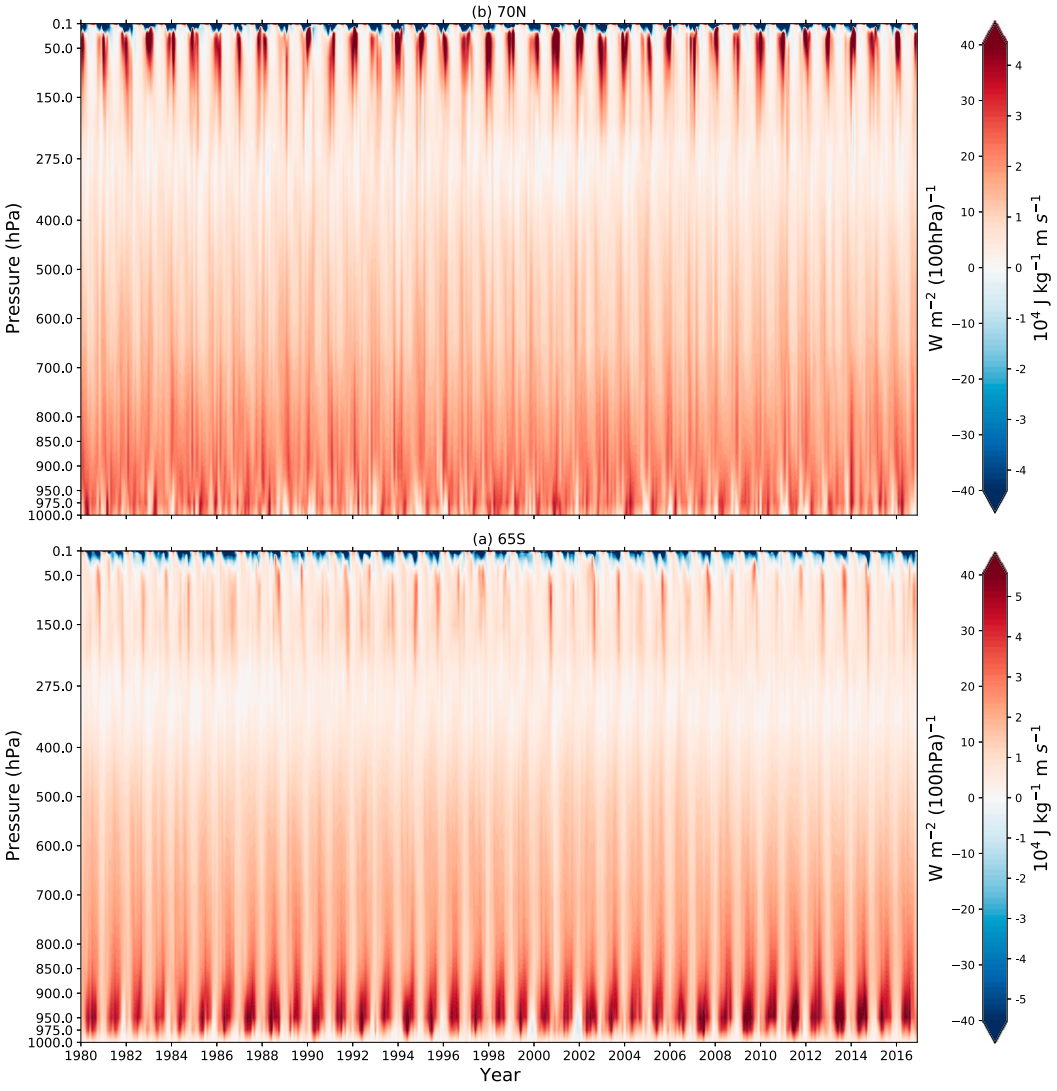

FIG. 1. Time–pressure series of monthly mean moist static energy flux (J kg^{-1} m s^{-1}) and local moist static energy flux convergence [W m^{-2} (100 hPa)$^{-1}$] across (a) 70°N and (b) 65°S with positive defined as a poleward flux.

summer stratospheric flux. During the summer mean, Overland and Turet (1994) showed a maximum of approximately 10 W m^{-2} (100 hPa)$^{-1}$ in the MSE flux at 50 hPa, the top level of the GFDL dataset, while the flux is near 0 throughout much of the stratosphere using the MERRA-2 dataset, with a small local maximum around 200 hPa. The stratospheric maximum during the winter in the GFDL dataset is also slightly larger.

c. *Stratospheric contribution to F_{wall}*

The mean annual cycle of F_{wall} and contributions from the stratosphere (F_{strat}), troposphere (F_{trop}), LH, SH, and GP fluxes are shown in Fig. 3, with climatological values at 70°N and 65°S included in Tables 1 and 2, respectively. In this study, F_{wall} is expressed as the polar cap–averaged MSE flux convergence (in W m^{-2}) calculated as the zonally and vertically integrated poleward flux at 65°S and 70°N.

The F_{strat} contributions to F_{wall}, expressed in both W m^{-2} and as a percentage, in the annual and winter mean are larger at 70°N than at 65°S. In the annual mean, F_{strat} at 70°N is 14.4 W m^{-2} or 15% of F_{wall}. The value of F_{strat} is largest during the winter, with a mean of 20.9 W m^{-2} or 19% of F_{wall} and weakest during the summer, with a mean of 6.0 W m^{-2} or 7% of F_{wall}. The value of F_{strat} at 65°S is 9.7 W m^{-2} or 11% of F_{wall} in the annual mean, 7.1 W m^{-2} or 6% of F_{wall} in the winter mean, and 9.1 W m^{-2} or 15% of F_{wall} in the summer mean. The winter and summer seasons at 65°S include local minima in the annual cycle, with local maxima occurring in March and October (Fig. 3e). This is consistent with increased magnitude of stratospheric stationary waves associated with October final warming events in the Southern Hemisphere.

The F_{strat} contributions to F_{wall} seasonality are larger at 70°N than at 65°S. The seasonal cycles in F_{strat} and F_{trop} at 70°N are

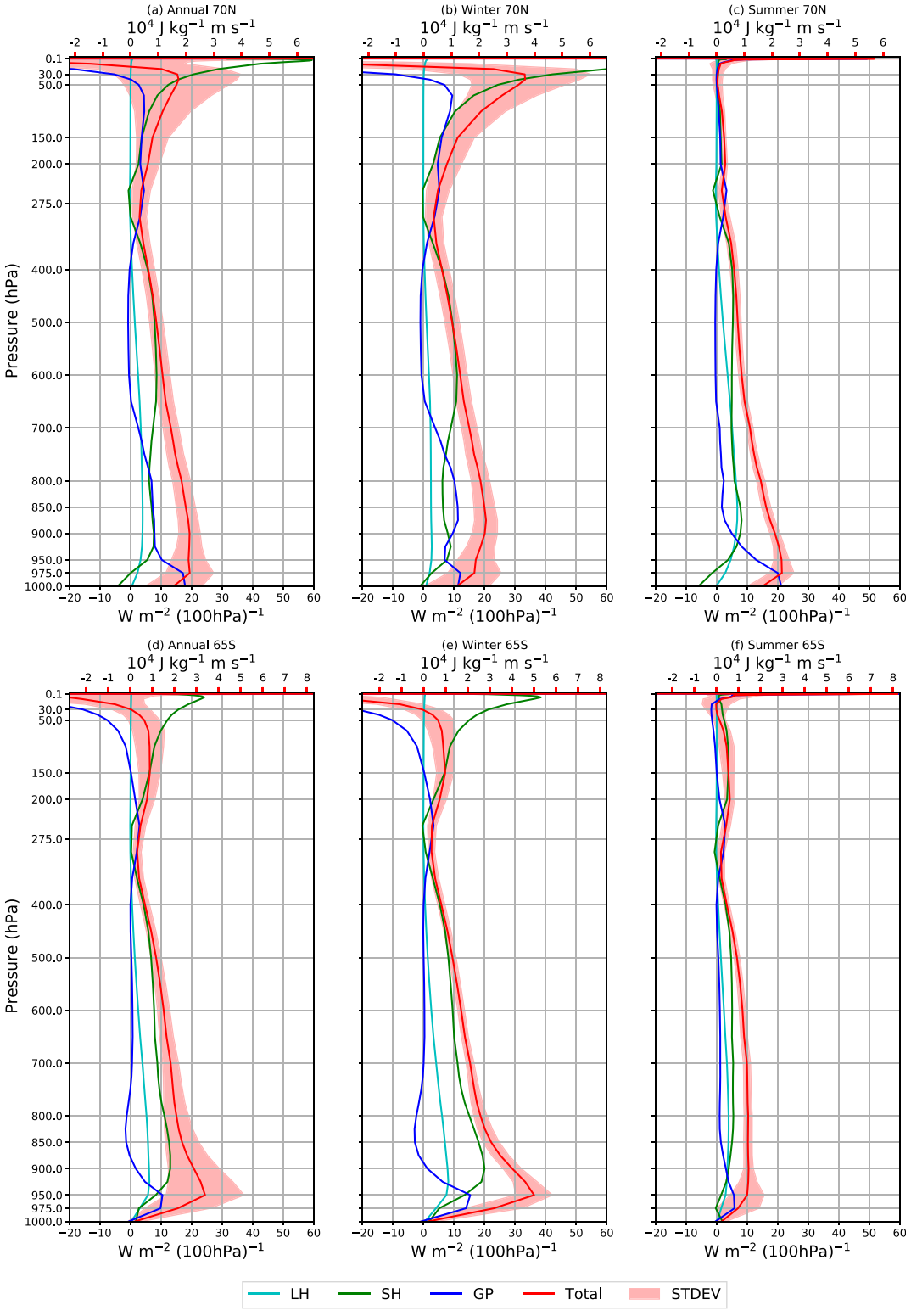

FIG. 2. Annual, winter, and summer mean local MSE flux convergence [red; W m^{-2} (100 hPa)$^{-1}$; lower axis], MSE flux (red; J kg^{-1} m s^{-1}; upper axis), and standard deviation (light red fill) across (a)–(c) 70°N and (d)–(f) 65°S with positive defined as a poleward flux. Contributions from the latent heat flux (LH; cyan), sensible heat flux (SH; green), and geopotential flux (GP; blue) are shown.

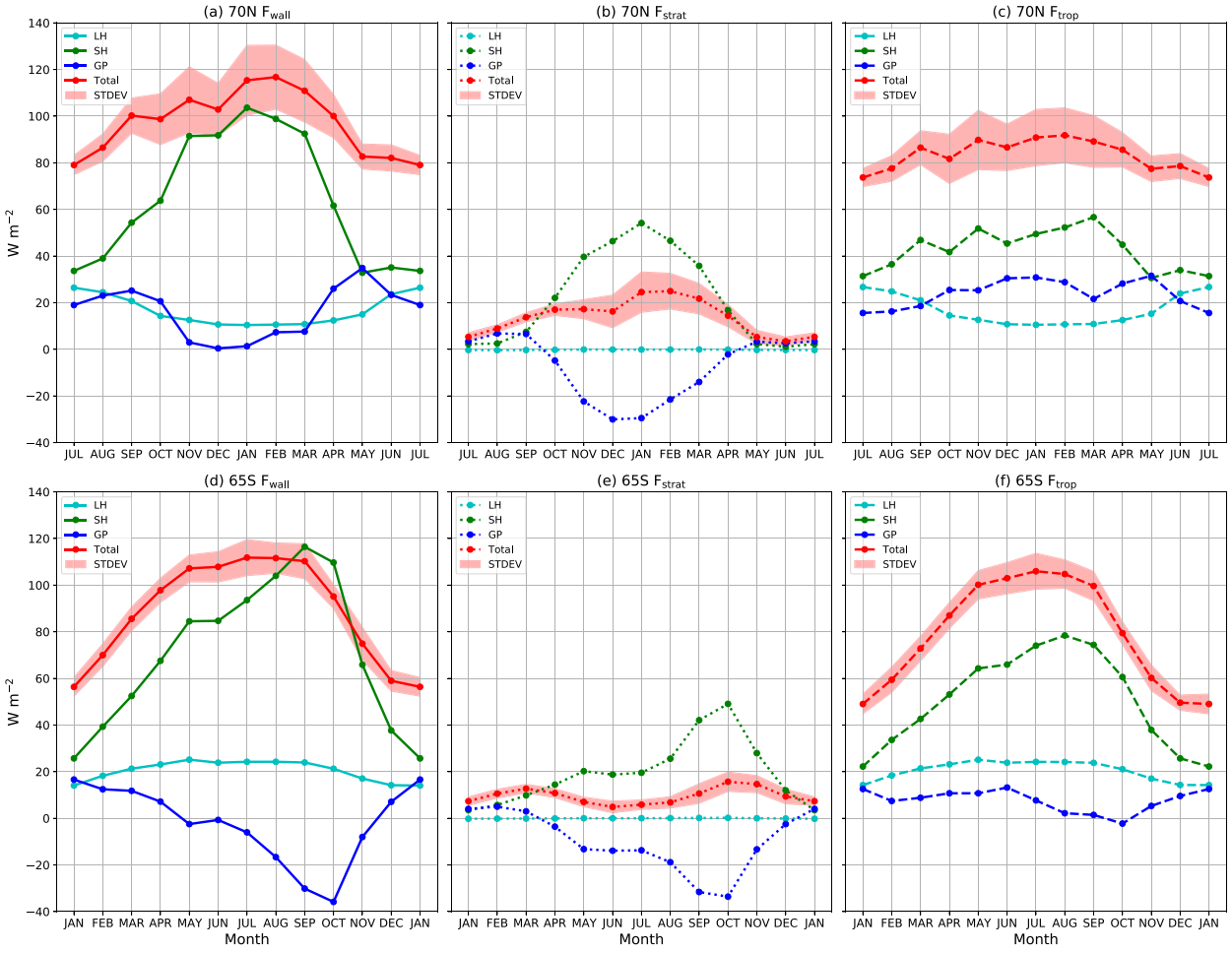

FIG. 3. Mean annual cycle of the vertically integrated, monthly, and polar cap–averaged flux convergence (F_{wall}; red), and contributions from the stratosphere (F_{strat}; dotted red) and troposphere (F_{trop}; dashed red), and standard deviation (light red fill) at (a)–(c) 70°N and (d)–(f) 65°S (W m^{-2}). Contributions from LH (cyan), SH (green), and GP (blue) are shown.

generally in phase. The seasonal range, defined as the maximum minus minimum monthly flux convergence derived from Fig. 3, is larger in F_{strat} (22 W m^{-2}) than in F_{trop} (18 W m^{-2}). Thus, at 70°N, F_{strat} contributes more to the seasonal range of F_{wall}. The SH component has the largest annual cycle in F_{wall}, which is best explained by its seasonality in the stratosphere (opposed in part by the GP component). The seasonal range of F_{wall} at 70°N is 32 W m^{-2} smaller than at 65°S. In general, the seasonal cycles in F_{strat} and F_{trop} at 65°S are out of phase. At 65°S, the seasonality of F_{wall} is dominated by F_{trop}, as there is little seasonality in F_{strat}, except in the largely opposed SH and GP components.

d. Variability of the stratospheric contribution to F_{wall}

Figure 4 shows the time series of monthly mean F_{wall}, F_{strat}, and F_{trop}. Interannual variability in F_{wall} is larger at 70°N than at 65°S, and F_{wall} is largest in both magnitude and variability during their respective winters, as can also be seen in Figs. 2 and 3.

Figure 5 shows the same monthly time series but expressed as anomalies relative to the mean annual cycle from Fig. 3. The variability of F_{strat} is larger in the Northern Hemisphere and explains more of the variance of F_{wall} than in the Southern Hemisphere. At 70°N, the Pearson correlation between F_{strat} and F_{trop} monthly mean anomalies is approximately zero during all seasons. However, the correlation between F_{strat} and F_{wall} anomalies is +0.48. In other words, F_{strat}, distinct from F_{trop}, explains 23% of the variance of F_{wall} at 70°N. During the summer, the correlation between F_{wall} and F_{strat} decreases to +0.33 (11% of the variance), and during the winter the correlation increases to +0.52 (27% of the variance). In contrast, at 65°S, F_{strat} only explains 10% of the variance of F_{wall}. Similar results are found at 70°N when using daily as opposed to monthly anomalies. These results show the importance of F_{strat} to F_{wall} variability at 70°N and a lesser degree of importance at 65°S. Section 4 will then focus on the variability of F_{strat} and F_{trop} at 70°N.

4. Link to the Arctic climate

a. Climate impacts of F_{strat} and F_{trop} anomalies

Given the vertical separation and temporal orthogonality of F_{trop} and F_{strat} anomalies seen in section 3d, we now ask if F_{trop}

TABLE 1. Climatological values of the vertically integrated polar cap–averaged moist static energy (MSE) flux convergence (F_{wall}) and contributions from the stratosphere (F_{strat}; 300–0.1 hPa) and troposphere (F_{trop}; 1000–300 hPa) for annual and seasonal means (W m^{-2}) at 70°N. Also provided are contributions from the sensible heat (SH), latent heat (LH), and geopotential (GP) flux convergence.

	Annual	Winter (DJF)	Spring (MAM)	Summer (JJA)	Fall (SON)	5-month winter (NDJFM)
F_{wall}	98.4	111.5	97.8	82.6	102.0	110.5
SH	66.3	98.0	62.3	35.9	69.8	95.6
LH	16.1	10.6	12.7	24.9	15.9	11.0
GP	16.0	2.9	22.8	21.8	16.3	3.9
F_{trop}	84.0	89.7	84.0	76.6	85.9	89.6
SH	43.3	48.9	44.0	33.9	46.7	51.1
LH	16.3	10.7	12.9	25.2	16.1	11.1
GP	24.4	30.1	27.1	17.5	23.1	27.4
F_{strat}	14.4	21.8	13.8	6.0	16.1	20.9
SH	23.0	49.1	18.3	2.0	23.1	44.5
LH	−0.2	−0.1	−0.2	−0.3	−0.2	−0.1
GP	−8.4	−27.2	−4.3	4.3	−6.8	−23.5

and F_{strat} anomalies have distinct climate impacts on the troposphere and stratosphere, respectively. To accomplish this task we analyze the signature of F_{wall} and its partitioning between F_{trop} and F_{strat} across composites of two different climate events: 1) sudden stratospheric warmings (SSWs) and 2) the atmospheric forcing of polar surface heating which we will quantify from downward surface flux events (DSFEs).

1) DEFINITION OF SUDDEN STRATOSPHERIC WARMINGS AND DOWNWARD SURFACE FLUX EVENTS

An SSW is defined as the first day on which the 60°N or 60°S $[u]_{10hPa}$ reverses from westerly to easterly during the winter (NDJFM in the Northern Hemisphere and MJJAS in the Southern Hemisphere). Additionally, $[u]_{10hPa}$ must return to westerly for at least 20 consecutive days between events. Table 3 lists these events, where the event date is defined as the central date (day of wind reversal). This definition of SSWs follows Charlton and Polvani (2007) except that, in this study, we include some early final warming events. These events are included because their dynamics are similar to midwinter SSWs; early final warmings tend to be strongly wave driven, and thus associated with greater heat flux than climatological or late final warmings (Butler et al. 2019). The event on 6 February 1995 is also not included in the MERRA-2 component of the SSW Compendium (Butler et al. 2017; Molod et al. 2015). This is likely due to only 1 day of easterlies during the event.

We expect that F_{strat} is anomalously poleward prior to the central date of an SSW and is preceded by poleward anomalies in F_{trop}. Polvani and Waugh (2004) showed that the 40-day period prior to the central date of SSWs is associated with anomalously strong poleward meridional eddy heat fluxes, averaged over the 40-day period, at 100 hPa. The meridional eddy heat flux at 100 hPa, which is averaged between 45° and 75°N in Polvani and Waugh (2004), is proportional to the eddy component of the SH term in F_{wall}. The meridional eddy heat flux is also proportional to the vertical component of the planetary wave activity flux (e.g., Edmon et al. 1980), with origins in the troposphere (e.g., Matsuno 1971; Polvani and Waugh 2004). The expected poleward anomalies in F_{trop} are associated with the tropospheric origin of SSWs, consistent with the weak but nonzero lagged correlation between monthly F_{trop} and F_{strat} anomalies, with F_{trop} leading by 1 month (+0.31). However, a near-tropopause-level (lower-stratospheric) planetary wave source may also play a role in the development of SSWs (Boljka and Birner 2020). The associated heat flux from a lower-stratospheric planetary wave source may not be well captured by F_{trop}.

TABLE 2. As in Table 1, but for 65°S.

	Annual	Winter (JJA)	Spring (SON)	Summer (DJF)	Fall (MAM)	5-month winter (MJJAS)
F_{wall}	90.7	110.4	93.4	61.6	96.8	109.8
SH	73.6	94.2	97.5	34.1	68.1	96.6
LH	20.9	24.1	20.7	15.5	23.2	24.3
GP	−3.8	−7.9	−24.8	12.0	5.5	−11.1
F_{trop}	81.0	104.6	79.8	52.5	86.6	102.7
SH	52.8	72.9	57.7	27.0	53.3	71.4
LH	20.9	24.1	20.6	15.6	23.2	24.2
GP	7.3	7.6	1.5	9.9	10.1	7.1
F_{strat}	9.7	5.8	13.6	9.1	10.2	7.1
SH	20.8	21.3	39.8	7.1	14.8	25.2
LH	0.0	0.0	0.1	−0.1	0.0	0.1
GP	−11.1	−15.5	−26.3	2.1	−4.6	−18.2

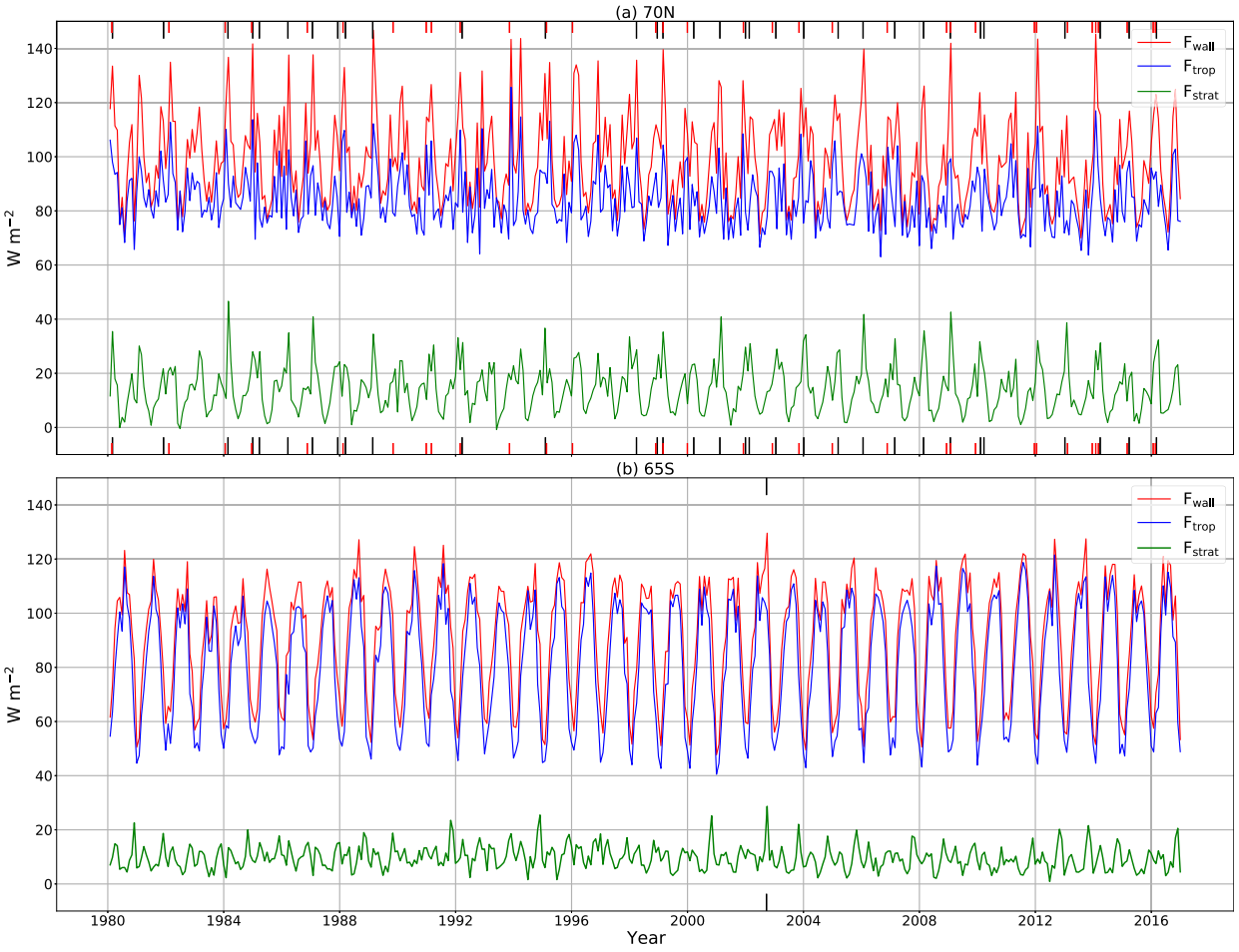

FIG. 4. Monthly mean F_{wall} (red), F_{strat} (green), and F_{trop} (blue) at (a) 70°N and (b) 65°S (W m^{-2}). Sudden stratospheric warmings (SSWs) are denoted by black tick marks, and downward surface flux events (DSFEs) for the Northern Hemisphere are denoted by red tick marks.

A DSFE is defined as the first day on which the surface downward energy flux averaged over the polar cap exceeds the 95th percentile threshold for the 5-month winter climatology. The net surface flux includes sensible and latent heat fluxes, the net longwave flux, and the absorbed shortwave flux, which is negligible during the winter. The central date of an event is defined as the day of the downward surface flux maximum. A 7-day rolling mean was applied to the surface flux data (3-hourly) to ensure that multiple maxima are not selected for one event. The linear trend was also removed from the surface flux data to ensure that events were selected over the entire dataset (red tick marks in Figs. 4 and 5). The 95th percentile threshold was chosen so that there are approximately the same number DSFEs (34) as SSWs (32).

We expect that F_{trop} is anomalously poleward prior to the central date of a DSFE. A downward surface flux indicates that the surface is warming at the expense of the atmosphere. During the winter, this is a combination of an increased downward longwave flux and suppression of upward sensible and latent heat fluxes, which is expected to be preceded by an increase in polar cap–averaged sensible and latent heat (moist enthalpy) in the troposphere.

2) COMPOSITE ANALYSIS OF SSWS AND DSFES

Table 4 shows composites of F_{wall}, F_{strat}, and F_{trop} in the 30-day mean before and after an SSW and DSFE. Both the raw flux convergence and anomalous flux convergence are provided to emphasize contributions to F_{wall}. We note that there is a small contribution (1–3 W m^{-2}) from the climatological seasonal cycle to the change in the raw flux convergence before and after an event. SSWs tend to occur later in the winter, while DSFEs tend to occur earlier in the winter; thus, there is a slight climatological decrease and increase in the flux convergence during SSWs and DSFEs, respectively. Prior to an SSW, there are statistically significant poleward anomalies in F_{wall} (12.2 W m^{-2}) primarily due to anomalies in F_{strat} (8.8 W m^{-2}). After the central date, statistically significant equatorward anomalies in F_{trop} and F_{wall} are found, possibly reflecting the lagged relationship between the stratosphere and troposphere during an SSW. Prior to a DSFE, there are statistically

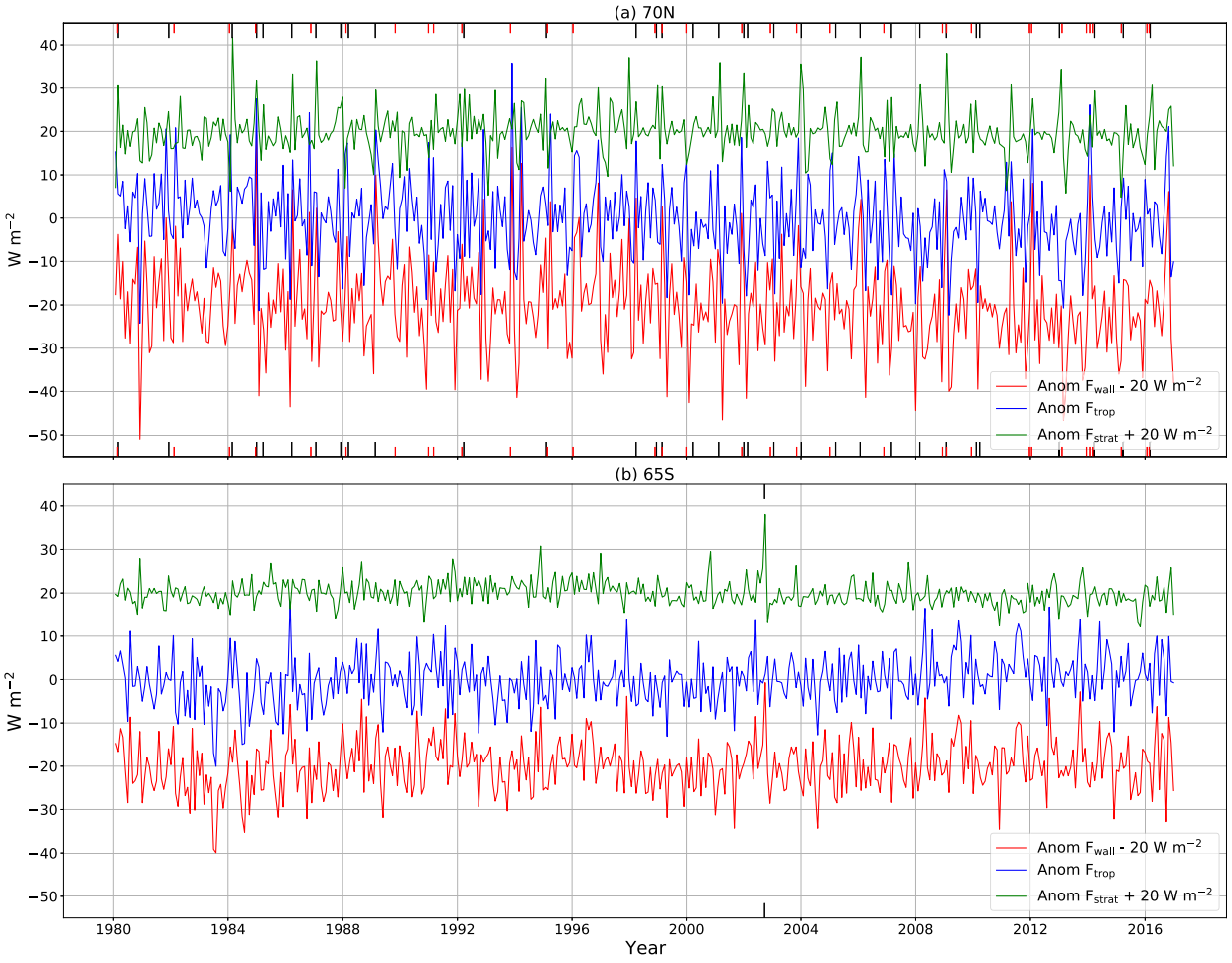

FIG. 5. Monthly mean anomalies in F_{wall} (red), F_{strat} (green), and F_{trop} (blue) at (a) 70°N and (b) 65°S (W m^{-2}). SSWs and DSFEs are denoted by black and red tick marks, respectively.

significant poleward anomalies in F_{wall} (7.6 W m^{-2}) primarily due to anomalies in F_{trop} (5.8 W m^{-2}). In other words, both types of events are preceded by significant poleward F_{wall} anomalies, with the anomalous heating located in the stratosphere and troposphere for SSWs and DSFEs, respectively.

To more precisely investigate the temporal evolution of the energy flux during SSWs and DSFEs, a composite of the daily mean F_{wall}, F_{strat}, and F_{trop} in the 30 days before and after these events are computed and are shown in Figs. 6a and 6c. The evolution of the stratosphere during SSWs includes two distinct periods associated with the weakening (breakdown) and strengthening (recovery) of the polar vortex centered around the central date. The period 30 days before and after the central date adequately captures the typical time scale of the deceleration of the zonal mean zonal winds (weakening) and the subsequent recovery of the polar vortex (black line in Fig. 6a). The observed increase in F_{strat} is largest in the 8 days prior to the central date. In that 8-day mean, the corresponding poleward F_{strat} anomaly is 25.2 W m^{-2}. The maximum anomaly in F_{strat} (37.2 W m^{-2}) on day −3 is preceded by a maximum anomaly in F_{trop} (20.5 W m^{-2}) on day −7. After the central date, F_{strat} returns to near climatology (cf. solid and dashed lines in Fig. 6a). This reduction is consistent with the decrease in meridional eddy heat flux anomalies after SSW events (e.g., Butler et al. 2017).

Figure 6b shows the vertical structure of the MSE flux convergence contributing to F_{wall} during an SSW. Compared to the winter climatology, anomalous poleward fluxes in the 8-day mean prior to the central date are found in the entire stratosphere. The maximum in the middle to upper stratosphere is significant prior to the SSW, with a relatively smaller increase with respect to the winter climatology in the middle troposphere. After the central date, much of the MSE flux in the column reduces to less than the winter climatology, with an exception in the lower troposphere. The composite of the 30-day mean after the SSW includes some dates in April (not included in the winter climatology), which is associated with the downward progression of the MSE flux convergence maximum and a climatological increase in the lower-tropospheric MSE flux convergence (Fig. 2). However, this lower-tropospheric increase is still anomalous with respect to the mean annual cycle.

A composite of DSFEs show the importance of F_{trop} anomalies in initiating these events (Fig. 6c). The observed

TABLE 3. Dates of sudden stratospheric warmings or weak vortex events. Dates of late-winter warmings not included in the MERRA-2 component of the SSW Compendium are denoted by an asterisk (*).

Year	Month	Day	Year	Month	Day
1980	Feb	29	2001	Feb	12
1981	Dec	04	2001	Dec	31
1984	Feb	24	2002	Feb	17
1985	Jan	01	2003	Jan	18
1985	Mar	25*	2004	Jan	05
1986	Mar	20*	2005	Mar	13*
1987	Jan	23	2006	Jan	21
1987	Dec	08	2007	Feb	24
1988	Mar	14	2008	Feb	22
1989	Feb	21	2009	Jan	25
1992	Mar	23	2010	Feb	09
1995	Feb	06	2010	Mar	24
1998	Mar	29*	2013	Jan	07
1998	Dec	16	2014	Mar	28*
1999	Feb	26	2015	Mar	28*
2000	Mar	20	2016	Mar	06*

increase in F_{trop} is largest in the 8 days prior to the central date, where a mean poleward anomaly of 36.5 W m^{-2} and a maximum anomaly of 47.9 W m^{-2} were found. After the central date, F_{wall} and F_{trop} reduce to approximately climatological levels. During the entire period, the anomalies in F_{strat} are not significantly different from zero.

Figure 6d shows the vertical structure of the MSE flux convergence during a DSFE. In the mean 8-day period prior to the central date of a DSFE, anomalous poleward fluxes compared to the winter climatology are found throughout the entire troposphere and are maximized in the lower troposphere. As suggested by the vertical structure, these events are associated with statistically significant poleward LH flux anomalies. In the 8-day mean prior to the central date, the contribution to the anomalous F_{trop} from the LH anomaly is 6.6 W m^{-2} (not shown). This is consistent with anomalous downward surface energy fluxes preceded by intense moisture flux events (Woods and Caballero 2016).

b. *Composite analysis of the Arctic response to SSWs and DSFEs*

In section 4a we analyzed the signature of F_{wall} and its partitioning into F_{strat} and F_{trop} across two different types of climate events: SSWs and DSFEs. This section focuses on the Arctic response to these two types of events.

Figure 7 shows composites of the anomalous energy budget of the Arctic climate system over SSWs (Fig. 7a) and DSFEs (Fig. 7b). The terms in the budget are cumulative time integrals of anomalous F_{wall}, F_{trop}, and F_{strat} and polar cap–averaged cumulative time integrals of anomalous moist enthalpy (h_m) tendency in the atmosphere (i.e., h_m storage—which is subdivided into stratospheric and tropospheric components), outgoing longwave radiation (OLR), and net surface flux (NSF) in MJ m^{-2}. The cumulative integration allows for easier visualization and starts 20 days before the central date of the

TABLE 4. Composite of the MSE flux convergence and associated MSE flux convergence anomalies (W m^{-2}) at 70°N averaged in the 30 days before and after the central date of an SSW and downward surface flux event (DSFE). An asterisk (*) indicates anomalies significantly different from zero at the 95% confidence level. A two-sided t test was used to determine significance. For p values < 0.05, we reject the null hypothesis of equal averages.

	Before central date		After central date	
	Flux convergence	Anomaly	Flux convergence	Anomaly
		SSWs		
F_{strat}	31.2	8.8*	20.6	−0.7
F_{trop}	94.3	3.4	82.7	−6.3*
F_{wall}	125.5	12.2*	103.3	−7.0*
		DSFEs		
F_{strat}	18.7	−1.8	23.9	2.3
F_{trop}	96.2	7.6*	88.7	−1.1
F_{wall}	114.9	5.8*	112.6	1.2

events, the approximate date when F_{wall} becomes anomalously poleward for an extended period. In Fig. 7, an increasing cumulative anomaly of a term indicates that there are positive anomalies of that term, with the slope indicating the magnitude of the anomaly on a particular lag day. Linear trends were removed for all anomalies in these composites.

In the SSW composite, first, there is a cumulative poleward increase in anomalous F_{strat} and associated stratospheric h_m storage. The increase in stratospheric h_m storage slows and subsequently decreases, indicating a gradual cooling. This stratospheric cooling is accompanied by a gradual increase in the cumulative OLR anomaly, with little change in the NSF. Cumulative F_{strat} is nearly balanced by the sum of h_m and OLR suggesting that the energy input by anomalous poleward F_{strat} during an SSW acts to increase the stratospheric h_m storage and OLR, with little influence on the surface. The total anomalous energy budget of the Arctic is not necessarily constrained in our analysis since all terms are calculated independently. However, the sum of all terms nearly balance in both the stratosphere and troposphere (see Fig. B1 in appendix B), suggesting that our analysis conserves energy in the column average, troposphere, and stratosphere. The NSF even becomes weakly anomalously upward (negative) after the central date, a response to equatorward F_{trop} anomalies. These results are fairly consistent with the SSW life cycle as explored by Limpasuvan et al. (2004). During the SSW life cycle, poleward heat flux anomalies found in the troposphere and stratosphere during the breakdown of the polar vortex are followed by equatorward heat flux anomalies in the troposphere during the recovery of the polar vortex.

In the DSFE composite (Fig. 7b), first there is a cumulative increase in the anomalous F_{trop} and associated tropospheric h_m storage. The increase in tropospheric h_m storage slightly precedes the increase in F_{trop} due to an anomalously upward NSF contributing energy to the troposphere at the beginning of the period. While the increasing tropospheric h_m storage anomaly slows and subsequently decreases (cooling and drying), there is a cumulative downward (positive) increase in the NSF

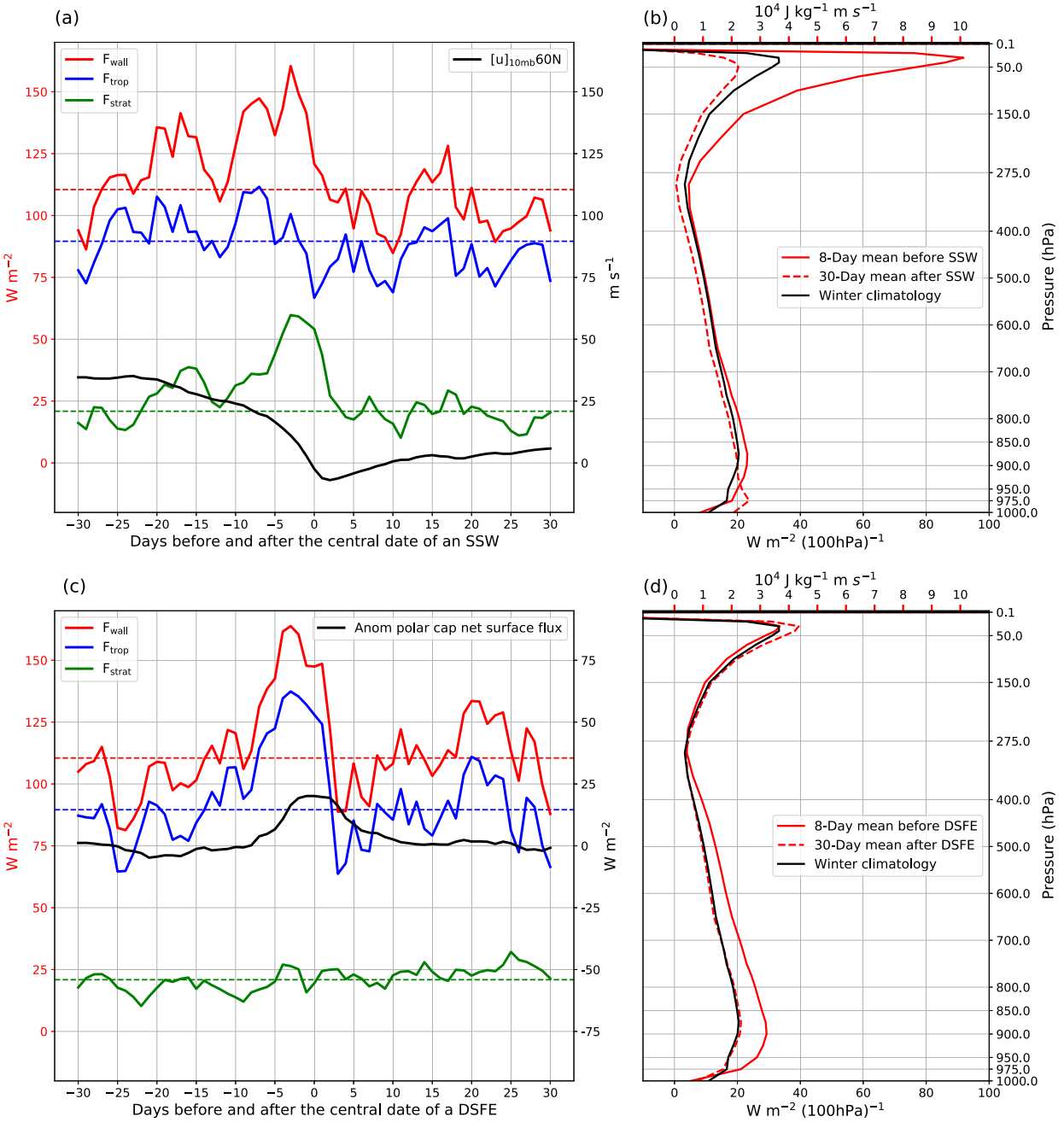

FIG. 6. (a) Composite of daily mean F_{wall} (red), F_{strat} (green), F_{wall} (blue), and associated winter climatologies (dashed) during SSWs or weak vortex events (32) at 70°N. Also shown is the composite of the daily mean $[u]_{10\text{hPa}}$ across 60°N (black). (b) Composite of the total MSE flux in the 8-day mean prior to the SSW central date (red solid), in the 30-day mean after the SSW central date (red dashed), the winter climatology of the total MSE flux (black) across 70°N ($\text{J kg}^{-1}\,\text{m s}^{-1}$), and the corresponding local flux convergence [W m^{-2} $(100\,\text{hPa})^{-1}$]. (c) As in (a), but for DSFEs (34). Also shown is a composite of the linearly detrended anomalous polar cap surface flux (positive downward; black). (d) As in (b), but for DSFEs.

anomaly. This composite shows that the energy input from F_{wall} primarily heats the atmosphere preceding the DSFE and this energy is subsequently fluxed downward from the warmed atmosphere to the surface. After the event is over, F_{wall} has returned to climatology and the anomalous F_{wall} over the duration of the event, almost entirely due to F_{trop}, has primarily gone into the surface (accumulated NSF), secondarily increased the energy content of the atmosphere, and only a small portion has been radiated back to space (little response in the OLR). The approximate budget closure in the troposphere and

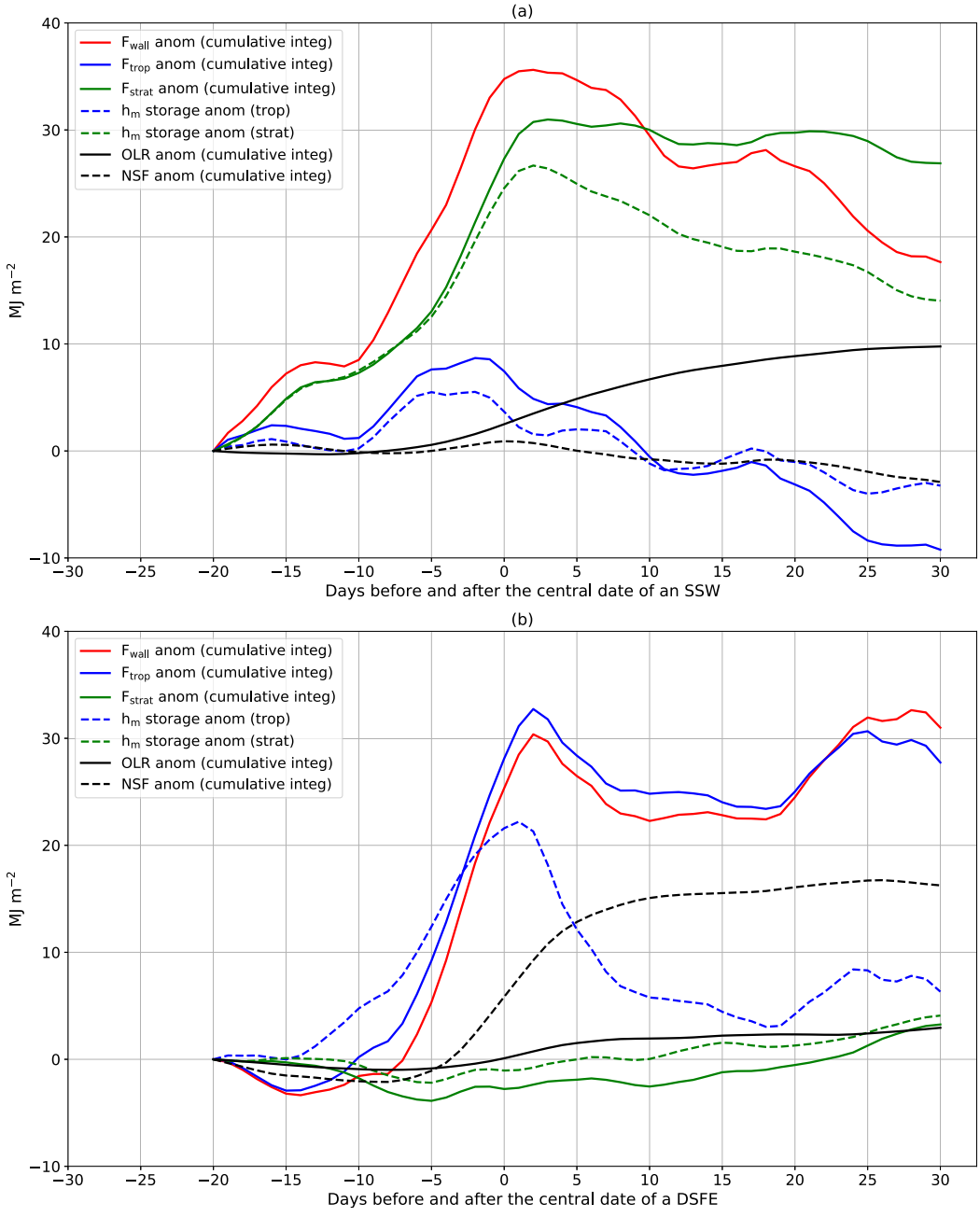

FIG. 7. (a) Composite of the cumulative time integral of anomalous F_{wall} (red), F_{strat} (green dashed), F_{trop} (blue dashed), outgoing longwave radiation (OLR; black dashed; positive upward), net surface flux (NSF; black dashed; positive downward), tropospheric moist enthalpy tendency (h_m storage; blue dashed), and stratospheric moist enthalpy tendency (h_m storage; green dashed) during SSWs (MJ m^{-2}). (b) As in (a), but for DSFEs. Anomalies are linearly detrended.

stratosphere suggests that the energy exchanges between stratosphere and troposphere within the polar cap are relatively small (see appendix B). A similar small vertical exchange of energy across the tropopause is found in other stratospheric events described in Dunn-Sigouin and Shaw (2015): strong vortex and extreme heat flux events (not shown).

The composite analysis shown in Fig. 7 suggests that the Arctic surface climate is more sensitive to F_{trop} than F_{strat} variability. In other words, F_{trop} is more efficient at warming the surface than F_{strat}. A schematic of the response to an anomalous increase in F_{strat} and F_{trop} is shown in Fig. 8. Although both events are associated with a similar increase in

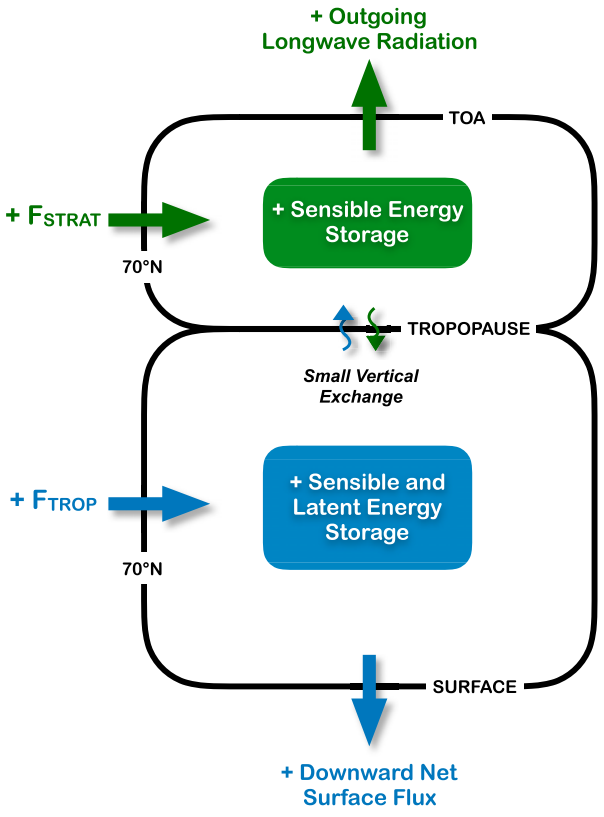

FIG. 8. Schematic of the response to an increase in the stratospheric (F_{strat}) and tropospheric (F_{trop}) flux convergence in the Arctic polar cap poleward of 70°N. The response to an increase in F_{strat} (green) is an increase in the stratospheric sensible energy storage followed by an increase in outgoing longwave radiation (OLR). The response to an increase in F_{trop} (blue) is an increase in the tropospheric sensible and latent energy storage followed by an increase in the downward net surface flux (NSF). Note that there is a relatively small vertical exchange across the tropopause.

F_{wall}, the NSF term only shows a large anomalous response when F_{wall} is dominated by F_{trop}. Although not reflected in the surface energy budget of the Arctic, these results do not suggest that SSWs have no climatic impact as surface impacts can result from dynamical stratosphere–troposphere coupling (Kidston et al. 2015). In addition, individual SSW events might show a more pronounced lagged relationship between F_{strat}, F_{trop}, and the NSF.

c. *Metric for the influence of atmospheric circulations on the Arctic surface climate*

Results thus far have shown that F_{strat} is an important contributor to F_{wall} variability into the Arctic and that a poleward increase in F_{strat} does not result in increased area-averaged heat flux to the Arctic surface. Accordingly, F_{trop} should then be a better metric for the influence of atmospheric circulations on the Arctic surface climate than F_{wall}, especially during the winter when F_{strat} variability is largest. Figure 9 shows correlations between the lower-tropospheric (1000–900 hPa) polar cap–averaged h_m tendency, F_{wall}, and F_{trop}. Correlations are plotted with respect to rolling means, applied to all data, up to 30 days. Correlations between F_{trop} and the h_m tendency are indeed larger than the correlations with F_{wall}, especially during the winter. Thus, F_{trop} explains a larger proportion of the variance of the h_m tendency. This result is quantitatively similar to the proportion of F_{wall} variance explained by F_{strat} provided in section 3d.

During the 1980–2016 period considered in this data, the maximum correlation for any rolling mean window is larger when using F_{trop} as opposed to F_{wall}. For the full dataset, the maximum correlation increases from 0.64 to 0.75, during the winter the maximum increases from 0.64 to 0.76, and during the summer the maximum increases from 0.64 to 0.71. During the summer, the maximum correlation between F_{trop} and the h_m tendency occur at a later rolling mean (11 days) than the winter (7 days) and correlations remain relatively high for longer time scales. One possible explanation for this result is that the ice albedo feedback results in a longer time scale of atmospheric response as the sea ice melts and additional solar energy is added to the Arctic climate system. During the winter, the coefficient of determination (correlation squared) increases from 0.41 to 0.58. Therefore, F_{wall} explains 17% more of the variance of the h_m tendency when F_{strat} is filtered out.

5. Conclusions and discussion

In this analysis, the vertical structure of the poleward moist static energy (MSE) flux in the MERRA-2 across 70°N and 65°S was examined. Our study sought to quantify the stratospheric (F_{strat}) and tropospheric (F_{trop}) contributions to F_{wall}, and the Arctic response following events of significant increases in F_{strat} and F_{trop}. In both hemispheres, local maxima in magnitude and variability of the poleward MSE flux are found at two vertically distinct locations in the middle to upper stratosphere and middle to lower troposphere with a minimum near the tropopause. The F_{wall} term is separated into distinctly stratospheric and tropospheric components that have temporally uncorrelated anomalies. Notably, F_{strat} was found to be nonnegligible, especially at 70°N during winter (NDJFM), where F_{strat} contributes 19% of the climatological F_{wall}. The F_{strat} term distinctly explains 23% of the variance of F_{wall} when using monthly mean anomalies; this value provides an estimate of how much F_{strat} biases the part of F_{wall} that is relevant to the Arctic surface climate.

Motivated by the greater importance of F_{strat} variability to F_{wall} at 70°N, we focused on the Arctic and argued that F_{trop} and F_{strat} have different impacts on the climate system, with F_{trop} associated with energy input to the surface of the Arctic and F_{strat} associated with sudden stratospheric warmings (SSWs). Figure 8 provides a visual summary of the Arctic response to poleward anomalies in F_{trop} and F_{strat}. In the 20 days preceding an SSW, significant poleward F_{strat} anomalies lead to stratospheric warming, with the majority of the F_{strat} anomaly going into stratospheric sensible energy storage, approximately one-third of the energy input radiated to space, and little change in the net surface flux. During winters with early (December–January) SSWs, Kuttippurath and Nikulin (2012) found minimal wintertime stratospheric ozone loss (i.e.,

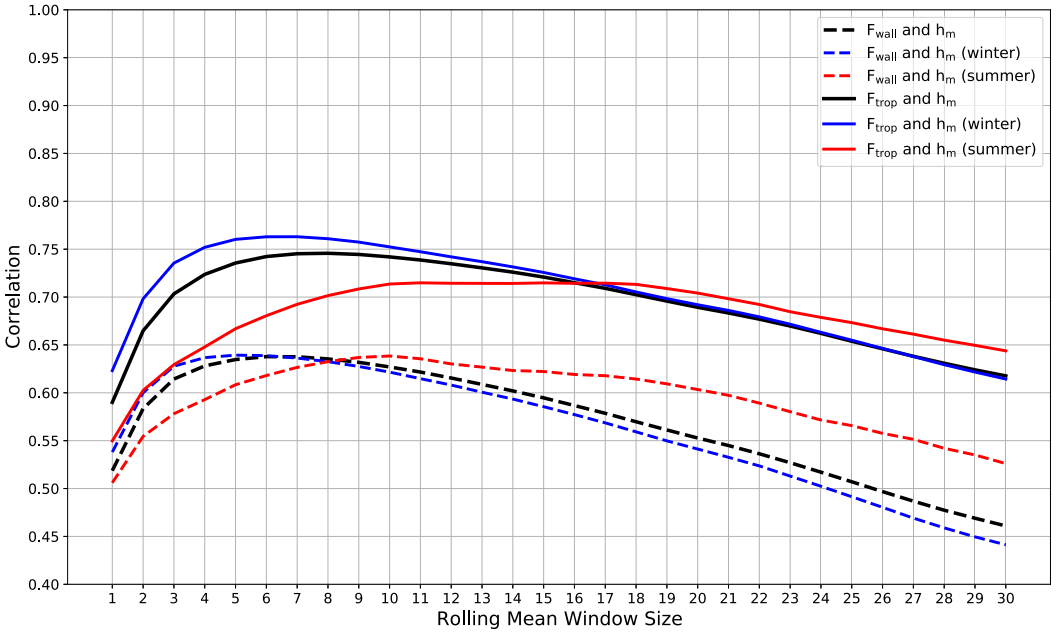

FIG. 9. Correlation between polar cap and lower-tropospheric (1000–900 hPa) averaged moist enthalpy (h_m) tendency, F_{wall} (dashed), and F_{trop} (solid), in the full dataset (black), winter (blue), and summer (red). Rolling means are applied to both the h_m tendency and energy convergence.

increased ozone concentrations). This increase in ozone concentrations is associated with increased atmospheric emissivity, which may play a role in the increased OLR along with the warmer temperatures, although we have not attempted to separate these signals.

In the 15 days preceding a downward surface flux event in the Arctic (DSFE), significant poleward F_{trop} anomalies lead to the heating and moistening of the atmospheric column. Thereafter, F_{trop} anomalies are not sustained and the warmed atmosphere fluxes energy downward with the net effect of the event being a near balance of the time-integrated F_{wall} anomaly and surface energy anomaly. Removing F_{strat} variability from F_{wall} resulted in an increased correlation between F_{wall} and the lower-tropospheric h_m (sensible and latent energy) tendency. Therefore, the efficiency with which poleward anomalies in F_{wall} warm the Arctic surface is increased during periods dominated by tropospheric anomalies. For a given poleward F_{trop} anomaly, the surface warming efficiency is expected to increase with pressure (lower-tropospheric heating) and with the contribution from the LH component. LH flux convergence is associated with both atmospheric heating and moistening (increased atmospheric emissivity), and thus an increased downward longwave flux to the surface (Graversen and Burtu 2016).

Our results suggest that, composited over many events, F_{strat} and F_{trop} variability is distinct (temporally orthogonal) and primarily impact the stratosphere (SSWs) and surface (DSFEs), respectively. These results, however, do not rule out the importance of troposphere–stratosphere interactions for individual events. There may exist events that, similar to events described in Baggett and Lee (2017), are associated with both large poleward anomalies in F_{wall} dominated by F_{trop} and high planetary wave activity. As a result of the increase in planetary wave activity, these events may be associated with a larger vertical exchange of energy across the tropopause than DSFEs and may precede some SSW events, which is consistent with the dynamical theory of SSWs. These events would likely be less efficient at warming the surface than DSFEs as a result of the larger troposphere to stratosphere energy flux.

We speculate that changes to the vertical structure of F_{wall} in a warmer climate will change the surface warming efficiency of F_{wall} in the Arctic due either to changes in F_{strat} or F_{trop}. Recent work has looked at changes in SSWs in transient climate change simulations, which could impact variability and trends in F_{strat}. Ayarzagüena et al. (2018) found no statistically significant changes in SSW frequency or duration by the end of the twenty-first century, across 12 Chemistry–Climate Model Initiative (CCMI) models. This result suggests that robust changes in the surface warming efficiency of F_{wall} will be linked to the troposphere. Comprehensive climate models project increased moisture transport (i.e., LH flux) into the Arctic under future global warming (Hwang and Frierson 2010), which is thought to be an important driver of polar amplification of climate change (e.g., Alexeev and Jackson 2013). Changes in total F_{wall} are anticorrelated with the amount of polar amplification, with the decrease in the flux of dry static energy dominating the intermodel spread in F_{wall} (Hwang et al. 2011). We speculate that these changes are associated with a downward shift toward a more tropospheric-weighted F_{wall} (since the LH component is all tropospheric, e.g., Fig. 3), which would increase the surface warming efficiency of F_{wall}. It is possible that this downward shift overwhelms any effects of

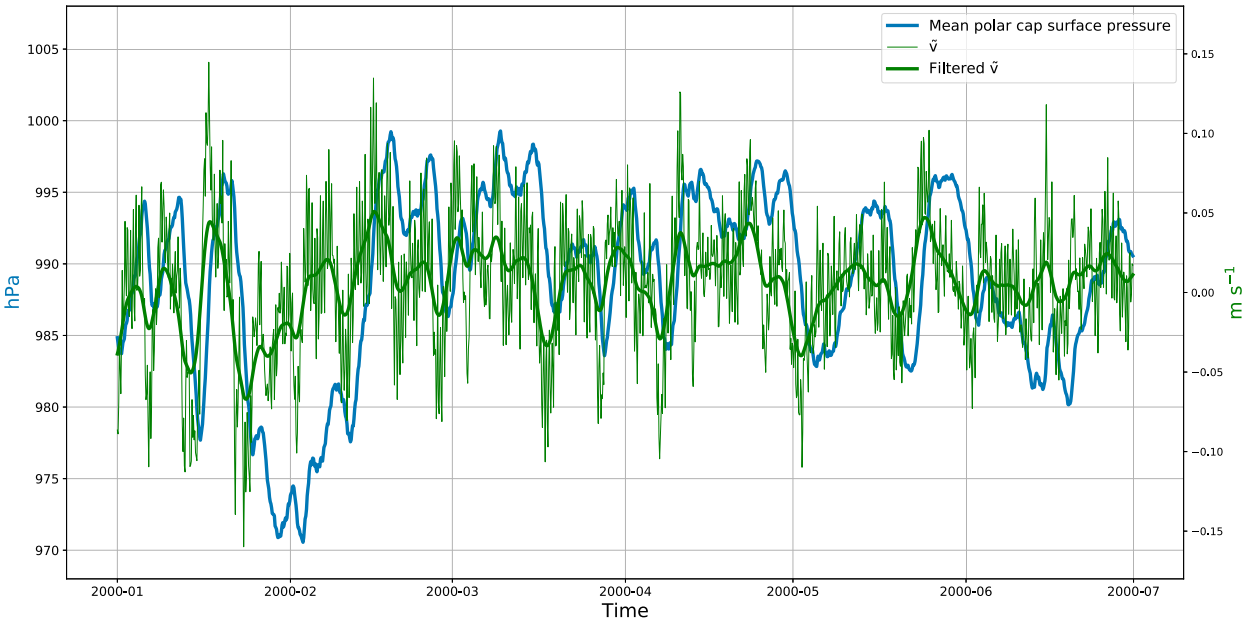

FIG. A1. 3-hourly instantaneous polar cap–averaged surface pressure (blue; hPa), $\tilde{v}$ at 70°N (light green), and low-pass filtered $\tilde{v}$ with a cutoff time scale of 4 days (green) between January 2000 and July 2000.

changes in total F_{wall}, and this may be an underappreciated mechanism for polar amplification.

To better understand the relationship between the poleward energy flux and polar amplification, future work will focus on the changes in F_{wall} efficiency in a warmer climate associated with changes in the vertical structure of F_{wall}, including the likely complex causal relationships between F_{wall} structure, Arctic stratification, and sea ice loss.

Acknowledgments. We thank three anonymous reviewers for their detailed comments, which helped reframe and improve our study. C.J.C. and B.E.J.R. were supported by NSF Award AGS-1455071, A.L.L. was supported by NSF Award AGS-1547814, and A.D. was supported by NSF Antarctic Program Grant Number PLR 1643436 and the NOAA MAPP Grant eGC1#A127135.

Data availability statement. The MERRA-2 data used in this study have been provided by the Global Modeling and Assimilation Office (GMAO) at NASA Goddard Space Flight Center through the Goddard Earth Sciences (GES) Data and Information Services Center (DISC) archive (GMAO 2015). The code to reproduce the results is available at https://github.com/cjcardinale/Cardinale-et-al-2021-JCLI.

APPENDIX A

F_{wall} Decomposition and Quantifying the Net Mass Flux

The components of the moist static energy (MSE) flux, sensible heat flux (SH), latent heat flux (LH), and geopotential flux (GP), can be expanded into an eddy flux (EF), a mean meridional circulation flux (MMC), and a net mass flux (NMF). For example, the SH term can be expanded as

$$\underbrace{c_p[(v)(T)]}_{\text{SH}} = \underbrace{c_p[(v^*)(T^*)]}_{\text{EF}} + \underbrace{c_p[(v)''(T)'']}_{\text{MMC}} + \underbrace{c_p\tilde{v}\tilde{T}}_{\text{NMF}}, \tag{A1}$$

where

$$\underbrace{[b] \equiv \frac{1}{2\pi}\int_0^{2\pi} b\,d\lambda}_{\text{zonal mean}},$$

$$\underbrace{\{b\} \equiv \frac{1}{\int dp/g}\int b\,dp/g}_{\text{mass weighted vertical average}},$$

$$\underbrace{b^* \equiv b - [b]}_{\text{departure from zonal mean}},$$

$$\underbrace{b'' \equiv b - \{b\}}_{\text{departure from mass weighted vertical average}},$$

and

$$\underbrace{\tilde{b} \equiv \frac{1}{\left[\int dp/g\right]}\left[\int b\,dp/g\right]}_{\text{zonal mean of the mass weighted vertical average}}.$$

The NMF is defined as the MSE brought into the polar cap via a net mass transport. The NMF has no vertical structure (i.e., all the information on the vertical structure of the MSE flux is contained in the EF and the MMC). The NMF is written in terms of the vertically and zonally averaged meridional wind $\tilde{v}$. This is in contrast to Overland and Turet (1994), where the

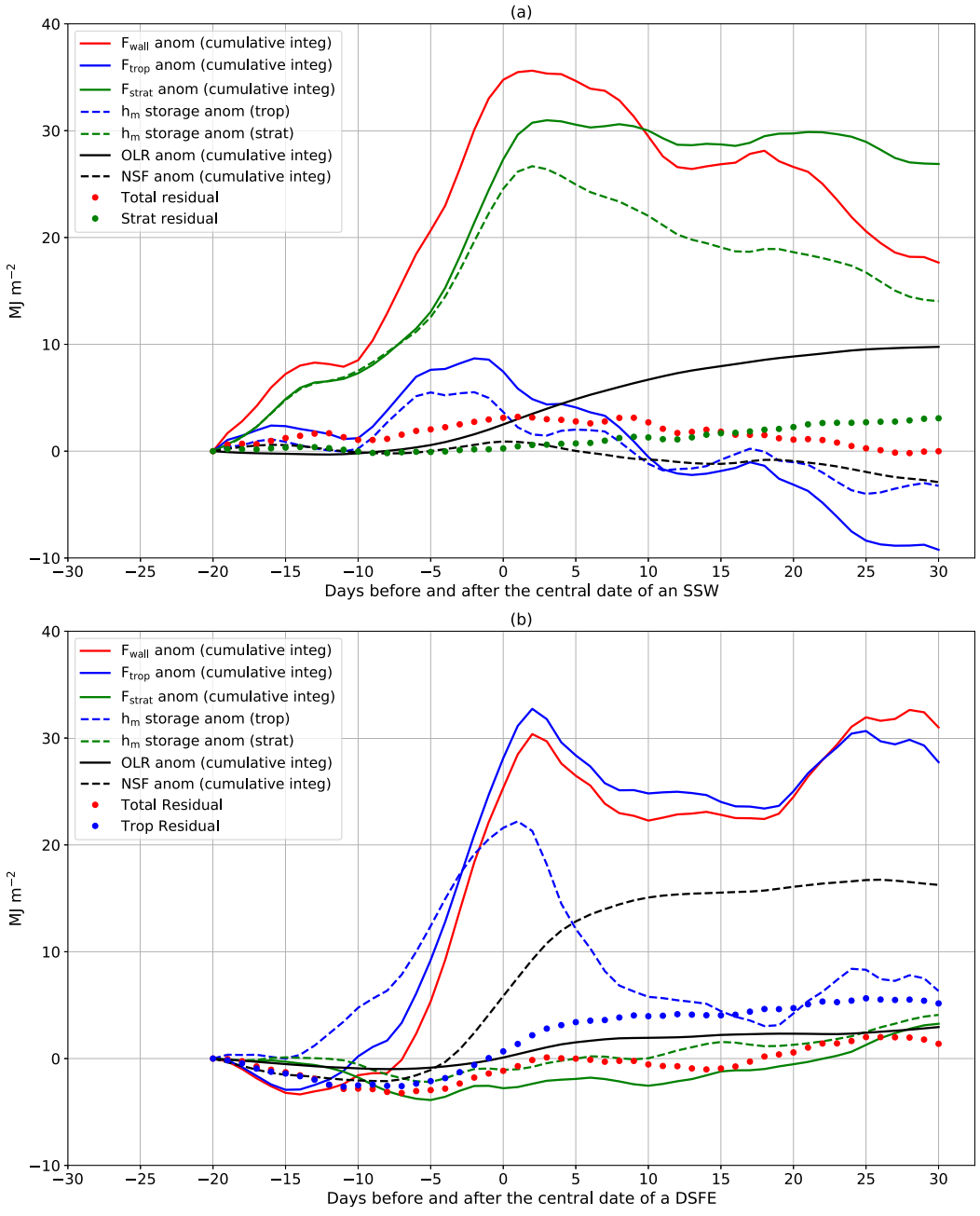

FIG. B1. As in Fig. 7, but with the energy budget residual in the total (dotted red), troposphere (dotted blue), and stratosphere (dotted green).

NMF term is $c_p[(\overline{v})][(\overline{T})]$ (the overline denotes a time average). Our definition of the NMF ensures that a longitude with relatively high terrain contributes less to the NMF.

The NMF term has been removed from F_{wall} calculations due to unphysical high-frequency noise. The $\tilde{v}$ term (proportional to the NMF) has been subtracted from v for the entire dataset to ensure mass balance and remove the NMF. Figure A1 shows the 3-hourly instantaneous polar cap–averaged surface pressure and the correction to the meridional wind (v) that removes the NMF for the period January–July 2000. If $\tilde{v}$ is a physical signal, then it should be well correlated with the surface pressure. A correlation of 0.48 is found for the year 2000 across 70°N at a lag of about 1 day. Also shown is the low-pass filtered $\tilde{v}$, with a cutoff time scale of 4 days. The correlation between the surface pressure and the filtered $\tilde{v}$ is 0.65 at a lag of 1 day. We then conclude that there is a decent amount of high-frequency noise associated with $\tilde{v}$ and the NMF. This noise may be associated with interpolation of the data to regular pressure

levels. This contrasts with the Overland and Turet (1994) method of assuming that for monthly time averages $[(\bar{v})] \approx 0$, a method that would remove any low-frequency signal while retaining the high-frequency signal. In addition, Liang et al. (2018) showed that a majority of the MSE brought to the polar caps through high-frequency net mass transport does not increase the average energy of the polar caps. The increase in the energy storage of the polar cap is exactly balanced by the added mass for air masses at the same energy as the polar cap.

The mean and variability of $\tilde{v}$ implies a large contribution from the NMF to F_{wall} in the dataset. The value of $\tilde{v}$ at 70°N for the entire dataset is $0.006\,\text{m s}^{-1}$ and is $-0.004\,\text{m s}^{-1}$ at 65°S, indicating a small poleward and equatorward flux of mass, respectively. Root-mean-square deviation (RMSD) between $\tilde{v}$ and the corrected $\tilde{v}$ ($0\,\text{m s}^{-1}$) at 70°N using the entire dataset is $0.04\,\text{m s}^{-1}$. At 65°S, the RMSD is also $0.04\,\text{m s}^{-1}$. Consider the NMF component of the SH term for a vertically averaged temperature of 250 K at 70°N. Although the mean ($0.006\,\text{m s}^{-1}$) and variability (given an RMSD of $0.04\,\text{m s}^{-1}$) of $\tilde{v}$ both appear small, they correspond to a NMF convergence mean and variability of 14 and 91 W m^{-2}, respectively. The NMF would have a much smaller contribution to F_{wall} if it were instead defined relative to the vertically averaged temperature of the polar cap (e.g., no contribution from the NMF component of the SH term convergence to F_{wall} for a polar cap–averaged temperature equal to the temperature at 70°N). This example points out both the sensitivity of F_{wall} to the definition of the NMF and the difficulty of physically interpreting this term (Mayer et al. 2019).

Applying a low-pass filter to $\tilde{v}$ and, as suggested by Liang et al. (2018), defining the NMF relative to the average energy of the polar caps would lead to a stronger correlation between the NMF and climate signals (e.g., the polar cap–averaged temperature tendency).

APPENDIX B

Energy Budget Residuals

Figure B1 shows composites of SSWs (Fig. B1a) and DSFEs (Fig. B1b) as in Fig. 7, but includes the energy budget residual in the total, troposphere, and stratosphere in MJ m^{-2}. The total residual is the difference between the energy input (F_{wall}), and Arctic response terms: net surface flux (NSF), outgoing longwave radiation (OLR), and total moist enthalpy (h_m) storage, with positive values indicating excess F_{wall}. The total residual could result from interpolation error, neglecting the contribution to F_{wall} from the climatically relevant part of the net mass flux (NMF), or energy imbalances in the underlying MERRA-2 data. The total residual indicates a slight excess of F_{wall} in the SSW composite (Fig. B1a) and, for most of the period, a slight deficit of F_{wall} in the DSFE composite (Fig. B1b).

The stratospheric residual is the difference between F_{strat} and combined OLR and stratospheric h_m storage terms, while the tropospheric residual is the difference between F_{trop} and combined NSF and tropospheric h_m storage terms. These residuals provide an estimate of the vertical exchange of energy across the tropopause. In the SSW composite, the stratospheric residual gradually increases following poleward anomalies in F_{strat}, suggesting a flux of energy from the stratosphere to the troposphere. In the DSFE composite, the tropospheric residual increases, especially from days −5 to +5, following poleward anomalies in F_{trop}, suggesting a flux of energy from the troposphere to the stratosphere. The energy exchange across the tropopause appears to be larger during DSFEs. However, the exchange is small relative to the magnitude of F_{wall} and the dominant Arctic response to F_{wall} during SSWs and DSFEs. This justifies the simple two-box interpretation of the energy budget sketched in Fig. 8.

REFERENCES

Alexeev, V. A., and C. H. Jackson, 2013: Polar amplification: Is atmospheric heat transport important? *Climate Dyn.*, **41**, 533–547, https://doi.org/10.1007/s00382-012-1601-z.

Ayarzagüena, B., and Coauthors, 2018: No robust evidence of future changes in major stratospheric sudden warmings: A multi-model assessment from CCMI. *Atmos. Chem. Phys.*, **18**, 11 277–11 287, https://doi.org/10.5194/acp-18-11277-2018.

Baggett, C., and S. Lee, 2015: Arctic warming induced by tropically forced tapping of available potential energy and the role of the planetary-scale waves. *J. Atmos. Sci.*, **72**, 1562–1568, https://doi.org/10.1175/JAS-D-14-0334.1.

——, and ——, 2017: An identification of the mechanisms that lead to Arctic warming during planetary-scale and synoptic-scale wave life cycles. *J. Atmos. Sci.*, **74**, 1859–1877, https://doi.org/10.1175/JAS-D-16-0156.1.

Boljka, L., and T. Birner, 2020: Tropopause-level planetary wave source and its role in two-way troposphere–stratosphere coupling. *Wea. Climate Dyn.*, **1**, 555–575, https://doi.org/10.5194/wcd-1-555-2020.

Bosilovich, M. G., and Coauthors, 2015: MERRA-2: Initial evaluation of the climate. NASA Tech. Rep. NASA/TM-2015-104606, Vol. 43, 139 pp., https://gmao.gsfc.nasa.gov/pubs/docs/Bosilovich803.pdf.

Butler, A. H., J. P. Sjoberg, D. J. Seidel, and K. H. Rosenlof, 2017: A sudden stratospheric warming compendium. *Earth Syst. Sci. Data*, **9**, 63–76, https://doi.org/10.5194/essd-9-63-2017.

——, A. Charlton-Perez, D. I. Domeisen, I. R. Simpson, and J. Sjoberg, 2019: Predictability of Northern Hemisphere final stratospheric warmings and their surface impacts. *Geophys. Res. Lett.*, **46**, 10 578–10 588, https://doi.org/10.1029/2019GL083346.

Charlton, A. J., and L. M. Polvani, 2007: A new look at stratospheric sudden warmings. Part I: Climatology and modeling benchmarks. *J. Climate*, **20**, 449–469, https://doi.org/10.1175/JCLI3996.1.

Cronin, T. W., and M. F. Jansen, 2016: Analytic radiative-advective equilibrium as a model for high-latitude climate. *Geophys. Res. Lett.*, **43**, L24807, https://doi.org/10.1002/2015GL067172.

Dunn-Sigouin, E., and T. A. Shaw, 2015: Comparing and contrasting extreme stratospheric events, including their coupling to the tropospheric circulation. *J. Geophys. Res.*, **120**, 1374–1390, https://doi.org/10.1002/2014JD022116.

Edmon, H. J., B. J. Hoskins, and M. E. McIntyre, 1980: Eliassen-Palm cross sections for the troposphere. *J. Atmos. Sci.*, **37**, 2600–2616, https://doi.org/10.1175/1520-0469(1980)037<2600:EPCSFT>2.0.CO;2.

GMAO, 2015: MERRA-2 inst3_3d_asm_Np: 3d, 3-hourly, instantaneous, pressure-level, assimilation, assimilated meteorological fields, V5.12.4. Goddard Space Flight Center Distributed Active Archive Center, accessed July 2017, https://doi.org/10.5067/QBZ6MG944HW0.

Graham, R. M., and Coauthors, 2019: Winter storms accelerate the demise of sea ice in the Atlantic sector of the Arctic Ocean. *Sci. Rep.*, **9**, 9222, https://doi.org/10.1038/s41598-019-45574-5.

Graversen, R. G., and M. Burtu, 2016: Arctic amplification enhanced by latent energy transport of atmospheric planetary waves. *Quart. J. Roy. Meteor. Soc.*, **142**, 2046–2054, https://doi.org/10.1002/qj.2802.

——, T. Mauritsen, M. Tjernström, E. Källén, and G. Svensson, 2008: Vertical structure of recent Arctic warming. *Nature*, **451**, 53–56, https://doi.org/10.1038/nature06502.

Hwang, Y.-T., and D. M. W. Frierson, 2010: Increasing atmospheric poleward energy transport with global warming. *Geophys. Res. Lett.*, **37**, 449–457, https://doi.org/10.1029/2010GL045440.

——, ——, and J. E. Kay, 2011: Coupling between Arctic feedbacks and changes in poleward energy transport. *Geophys. Res. Lett.*, **38**, L17704, https://doi.org/10.1029/2011GL048546.

Kidston, J., A. A. Scaife, S. C. Hardiman, D. M. Mitchell, N. Butchart, M. P. Baldwin, and L. J. Gray, 2015: Stratospheric influence on tropospheric jet streams, storm tracks and surface weather. *Nat. Geosci.*, **8**, 433–440, https://doi.org/10.1038/ngeo2424.

Kuttippurath, J., and G. Nikulin, 2012: A comparative study of the major sudden stratospheric warmings in the Arctic winters 2003/2004–2009/2010. *Atmos. Chem. Phys.*, **12**, 8115–8129, https://doi.org/10.5194/acp-12-8115-2012.

Liang, M., A. Czaja, R. Graversen, and R. Tailleux, 2018: Poleward energy transport: Is the standard definition physically relevant at all time scales? *Climate Dyn.*, **50**, 1785–1797, https://doi.org/10.1007/s00382-017-3722-x.

Limpasuvan, V., D. Thompson, and D. Hartmann, 2004: The life cycle of the Northern Hemisphere sudden stratospheric warmings. *J. Climate*, **17**, 2584–2596, https://doi.org/10.1175/1520-0442(2004)017<2584:TLCOTN>2.0.CO;2.

Matsuno, T., 1971: A dynamical model of the stratospheric sudden warming. *J. Atmos. Sci.*, **28**, 1479–1494, https://doi.org/10.1175/1520-0469(1971)028<1479:ADMOTS>2.0.CO;2.

Mayer, M., S. Tietsche, L. Haimberger, T. Tsubouchi, J. Mayer, and H. Zuo, 2019: An improved estimate of the coupled Arctic energy budget. *J. Climate*, **32**, 7915–7934, https://doi.org/10.1175/JCLI-D-19-0233.1.

McCarty, W., L. Coy, R. Gelaro, A. Huang, D. Merkova, E. B. Smith, M. Seinkiewicz, and K. Wargan, 2016: MERRA-2 input observations: Summary and assessment. NASA/TM-2016-104606, Tech. Rep. Series on Global Modeling and Data Assimilation, Vol. 46, 51 pp., https://ntrs.nasa.gov/archive/nasa/casi.ntrs.nasa.gov/20160014544.pdf.

Molod, A., L. Takacs, M. Suarez, and J. Bacmeister, 2015: Development of the GEOS-5 atmospheric general circulation model: Evolution from MERRA to MERRA2. *Geosci. Model Dev.*, **8**, 1339–1356, https://doi.org/10.5194/gmd-8-1339-2015.

Nakamura, N., and A. H. Oort, 1988: Atmospheric heat budgets of the polar regions. *J. Geophys. Res.*, **93**, 9510–9524, https://doi.org/10.1029/JD093iD08p09510.

Overland, J. E., and P. Turet, 1994: Variability of the atmospheric energy flux across 70°N computed from the GFDL data set. *The Polar Oceans and Their Role in Shaping the Global Environment*, *Geophys. Monogr.*, No. 84, Amer. Geophys. Union, 313–325.

Park, D.-S. R., S. Lee, and S. B. Feldstein, 2015: Attribution of the recent winter sea ice decline over the Atlantic sector of the Arctic ocean. *J. Climate*, **28**, 4027–4033, https://doi.org/10.1175/JCLI-D-15-0042.1.

Park, H.-S., S. Lee, S.-W. Son, S. B. Feldstein, and Y. Kosaka, 2015: The impact of poleward moisture and sensible heat flux on Arctic winter sea ice variability. *J. Climate*, **28**, 5030–5040, https://doi.org/10.1175/JCLI-D-15-0074.1.

Peixoto, J. P., and A. H. Oort, 1992: *Physics of Climate*. American Institute of Physics, 520 pp.

Polvani, L. M., and D. W. Waugh, 2004: Upward wave activity flux as a precursor to extreme stratospheric events and subsequent anomalous surface weather regimes. *J. Climate*, **17**, 3548–3554, https://doi.org/10.1175/1520-0442(2004)017<3548:UWAFAA>2.0.CO;2.

Porter, D. F., J. J. Cassano, M. C. Serreze, and D. N. Kindig, 2010: New estimates of the large-scale Arctic atmospheric energy budget. *J. Geophys. Res.*, **115**, D08108, https://doi.org/10.1029/2009JD012653.

Serreze, M. C., A. P. Barrett, A. G. Slater, M. Steele, J. Zhang, and K. E. Trenberth, 2007: The large scale energy budget of the Arctic. *J. Geophys. Res.*, **112**, D11122, https://doi.org/10.1029/2006JD008230.

Trenberth, K. E., 1991: Storm tracks in the Southern Hemisphere. *J. Atmos. Sci.*, **48**, 2159–2178, https://doi.org/10.1175/1520-0469(1991)048<2159:STITSH>2.0.CO;2.

——, and A. Solomon, 1994: The global heat balance: Heat transports in the atmosphere and ocean. *Climate Dyn.*, **10**, 107–134, https://doi.org/10.1007/BF00210625.

Woods, C., and R. Caballero, 2016: The role of moist intrusions in winter Arctic warming and sea ice decline. *J. Climate*, **29**, 4473–4485, https://doi.org/10.1175/JCLI-D-15-0773.1.

Yang, X.-Y., J. C. Fyfe, and G. M. Flato, 2010: The role of poleward energy transport in Arctic temperature evolution. *Geophys. Res. Lett.*, **37**, L14803, https://doi.org/10.1029/2010GL043934.